CEAS-GNC-2024-089

EuroGNC Navigation Guidance Control CEAS Bristol, UK June 11th-13th 2024
University of BRISTOL ROYAL AERONAUTICAL SOCIETY AIAA

LPV Modeling and Autopilot Design for a Dual Pulse Tail Controlled Missile

Frederik Prochazka Diehl Defence GmbH & Co. KG, Fischbachstraße 16, Röthenbach a. d. Pegnitz, Germany. frederik.prochazka@diehl-defence.com

ABSTRACT

The linear, parameter varying (LPV) modeling and autopilot design for a high-agile surface-to-air missile is presented. Missile autopilot design poses a challenging task, because a wide flight envelope needs to be covered by the resulting controller while fulfilling robust stability and performance requirements at the same time. Furthermore, the dynamic behavior of the missile is highly nonlinear and dependent on rapidly changing variables like the Mach number and incidence angle. For the example of a dual pulse missile presented here relevant changes in mass and center of gravity, respectively, have an additional large influence on the dynamics. In this paper a quasi-LPV model is derived, which also takes these influences into account and thus approximates the nonlinear missile behavior over the entire flight envelope. The choice of scheduling variables is discussed and the quality of the approximation is examined. Based on the developed quasi-LPV model, an exemplary LPV autopilot design is presented and the robustness of the closed-loop system is assessed. The autopilot performance is demonstrated within a high-fidelity simulation environment.

Nomenclature

ψ, θ, ϕ	=	Euler angles (heading, pitch, roll)
p, q, r	=	body-fixed angular rates (roll, pitch, yaw)
X, Y, Z	=	translational force in body-fixed axes (x, y, z)
L, M, N	=	moment around body-fixed axes (x, y, z)
$C_{()}$	=	aerodynamic coefficient
a_x, a_y, a_z	=	body-fixed acceleration (axial, lateral, longitudinal)
α, β	=	angle of attack/sideslip
ϑ, φ	=	incidence angle/aerodynamic roll angle
T	=	thrust
m	=	mass
I_{xx}, I_{yy}, I_{zz}	=	moment of inertia around body-fixed axes (x, y, z)
ξ, η, ζ	=	virtual aerodynamic control inputs (aileron, elevator, rudder)
V	=	absolute velocity
Ma	=	Mach number
a	=	speed of sound
$\rho, \bar{q}$	=	ambient/dynamic pressure
S	=	missile reference area
d	=	missile reference length
h	=	altitude

1 Introduction

Autopilot design for modern high-agile missiles comes with the requirement to cover extended flight envelopes and increase missile performance. This translates to superior maneuverability, demanding robust stabilization at high incidences, and great agility. The latter requires fast and accurate tracking of commanded cross acceleration in the face of highly nonlinear and fast varying missile dynamics. The main sources for nonlinearities – besides the aerodynamics – are thrust misalignment, uncertainties in the control effectiveness as well as rapid changes in the missile mass, moments of inertia and center of gravity. This holds especially true for the example of an agile, dual pulse surface-to-air missile with extended range, which is considered in this contribution.

Classical autopilot designs implement a gain-scheduling strategy where controllers are synthesized for linear time-invariant (LTI) representations of the system dynamics, which are obtained from trim calculations and subsequent linearization of the nonlinear dynamics around the derived points of equilibria. The controller gains designed at those trim points are typically interpolated based on Mach number and possibly other physical quantities [1, 2]. Such classical applications have the disadvantage that stability and performance are only guaranteed in the vicinity of the chosen scheduling points. Nevertheless, robust control theory for LTI systems has been successfully used for industrial missile applications in the past. In [3] the robust autopilot design for a highly agile tail/thrust-vector controlled air-to-air missile is presented, with the single controller outputs being blended based on dynamic pressure. Ref. [4] describes the extension of the aforementioned autopilot concept to a high-agile tail/thrust vector controlled surface-to-air missile, where the controllers are designed at certain Mach numbers and scheduled over altitude. To increase robust stability guarantees, one would need to either increase the parameter uncertainties considered in the autopilot design to enlarge the operating region covered by single controllers, which would degrade the closed-loop performance. Alternatively, the number of scheduling points could be increased so that regions of guaranteed robustness are overlapping to a large extent, which can become a tedious task. Regardless, neither approach changes the basic shortcomings of classical gain scheduling mentioned above. That is why the area of linear, parameter varying (LPV) control has been receiving a lot of attention for some time. The state and output equations of an LPV system are given by

$$\begin{aligned} \dot{\boldsymbol{x}} &= \boldsymbol{A}(\boldsymbol{\theta})\boldsymbol{x} + \boldsymbol{B}(\boldsymbol{\theta})\boldsymbol{u} \\ \boldsymbol{y} &= \boldsymbol{C}(\boldsymbol{\theta})\boldsymbol{x} + \boldsymbol{D}(\boldsymbol{\theta})\boldsymbol{u} \end{aligned} \tag{1}$$

with the state vector $\boldsymbol{x}$, the inputs $\boldsymbol{u}$, the outputs $\boldsymbol{y}$ and the parameter vector $\boldsymbol{\theta}$. An LPV system can approximate the nonlinear behavior of a system along the parameter trajectory $\boldsymbol{\theta}$, which is itself a function of time. For a frozen value of $\boldsymbol{\theta}$ an LPV system reduces to a regular LTI one [5]. If a subset of the parameter vector belongs to the system's state space the equations (1) describe a quasi-LPV (qLPV) model, which is a special case of an LPV system [6]. The concept of qLPV models has first been introduced in [7] and is often encountered in aerospace applications, with the angle of attack α being typically considered as part of $\boldsymbol{\theta}$ in LPV missile models [5, 8]. There are different methods available to derive LPV models from a nonlinear system model. In [6] three common aproaches are presented, namely state transformation, function substitution and grid-based Jacobian linearization. Here, the latter will be used to generate a qLPV model from the nonlinear missile dynamics.

When it comes to controller design the major advantage over classical gain scheduling is that LPV controller synthesis techniques provide explicit stability and performance guarantees in the face of parameter-varying system dynamics and uncertainties [9]. The basis for LPV autopilot design is the formulation of control problems as linear matrix inequalities (LMI), which can be solved by readily available algorithms [10]. The resulting controller $\boldsymbol{K}(\boldsymbol{\theta})$ is thus synthesized in a single step and is itself an LPV system, with the vector $\boldsymbol{\theta}$ assumed to be measurable. That means that the scheduling of the controller is implicitly performed during the design procedure and comes with robustness guarantees over the considered operating region, which is why LPV controllers are sometimes labeled as self-scheduled controllers [11]. Another advantage is that the LPV controller design framework can be seen as a direct extension of the

well-known $\mathcal{H}_\infty$ robust control design techniques [12]. For parameter-varying controller design the performance requirements are specified by the induced $\mathcal{L}_2$-norm, which is a generalization of the $\mathcal{H}_\infty$ norm [13, 14]. A few years ago the software collection *LPVTools* has been released, which contains all necessary functions for LPV controller synthesis in *MATLAB* [10]. The underlying algorithms are based on the results from [13, 14] and allow for the incorporation of rate bounds on the parameter vector $\boldsymbol{\theta}$, which can lead to a less conservative design as the controller does not need to fullfill the requirements over an infinite parameter space.
Here, the LPV modeling and controller design for an agile dual pulse tail controlled surface-to-air missile is presented. In contrast to other works in this field, where only the endgame phase with a burnt out missile is considered (see. e.g. [8, 11, 15]), the presented work explicitly considers the change of dynamics which is mainly due to loss of mass and center of gravity shift. To the author's knowledge this is the first work to consider these relevant effects in the design of a missile LPV model and autopilot design. In section 2 the missile model will be presented and a grid-based quasi-LPV model is derived and compared to the nonlinear missile's behavior. In section 3 the design of an LPV controller for the missile longitudinal axes is described. The robustness of the closed control loop is analyzed in section 4 and nonlinear simulation results are presented. The paper ends with a discussion and outlook on future works in section 5.

2 Missile Modeling

In this section the quasi-LPV model of the missile dynamics will be derived. First, basic modeling assumptions will be given and the nonlinear equations of motion of the missile model are presented. Then, the linearized missile dynamics will be analyzed and the choice for scheduling parameters in the vector $\boldsymbol{\theta}$ is given. Finally, the quality of the derived qLPV model of the missile is assessed by comparison with open-loop step responses of the nonlinear missile dynamics.

2.1 Nonlinear Missile Model

The nonlinear missile dynamics considered here are described by a 6 degree of freedom (6DOF) model, mostly following the typical assumptions made for rigid-body aerospace systems which can be found in [16]. These include the motion over a flat-earth, so that a local north-east-down coordinate system can be considered as an inertial reference frame (index i). In addition, the influence of wind is neglected ($\boldsymbol{V}_\mathrm{w} = \boldsymbol{0}$), causing the kinematic and aerodynamic velocities to coincide and thus eliminating the need for extra marking of translational and angular velocites. By applying Newton's second law of motion to the conservation of mass and angular momentum the missile's dynamic state equations during boost, expressed in body-fixed axes (index b), are given by

$$\dot{\boldsymbol{v}}^b = \frac{1}{m}(\boldsymbol{F}_\mathrm{A}^b + \boldsymbol{F}_\mathrm{T}^b + \boldsymbol{F}_\mathrm{G}^b) - \boldsymbol{\omega}_{b/i}^b \times \boldsymbol{v}^b \tag{2}$$

$$\dot{\boldsymbol{\omega}}_{b/i}^b = \boldsymbol{I}^{-1}(\boldsymbol{M}_\mathrm{A}^b + \boldsymbol{M}_\mathrm{T}^b + \boldsymbol{M}_\mathrm{J}^b - \boldsymbol{\omega}_{b/i}^b \times \boldsymbol{I}\boldsymbol{\omega}_{b/i}^b) \tag{3}$$

with the vector of body-fixed velocity components $\boldsymbol{v}^b = \begin{bmatrix} u & v & w \end{bmatrix}^\mathrm{T}$ and angular rates of the missile body relative to the inertial frame $\boldsymbol{\omega}_{b/i}^b = \begin{bmatrix} p & q & r \end{bmatrix}^\mathrm{T}$. External forces and moments acting at the center of gravity (cg) are due to aerodynamics (A), thrust (T), gravity (G) and jet damping (J). The latter effect is proportional to the mass flow rate and change in inertia and is based on the Coriolis effect through the burning rocket motor. While (2) is adequate for simulation purpose an alternative formulation of the translational motion is employed to derive the linearized short-period missile dynamics later on. This

alternative representation results from evaluating Newton's second law in aerodynamic axes (index a)

$$\begin{aligned}\dot{V} &= \frac{X_{\mathrm{A}}^a + X_{\mathrm{T}}^a + X_{\mathrm{G}}^a}{m} \\ \dot{\beta} &= \frac{Y_{\mathrm{A}}^a + Y_{\mathrm{T}}^a + Y_{\mathrm{G}}^a}{mV} + p \cdot \sin(\alpha) - r \cdot \cos(\alpha) \\ \dot{\alpha} &= \frac{Z_{\mathrm{A}}^a + Z_{\mathrm{T}}^a + Z_{\mathrm{G}}^a}{mV\cos(\beta)} + q - \tan(\beta)(p \cdot \cos(\alpha) + r \cdot \sin(\alpha))\end{aligned} \tag{4}$$

which leads to a state transformation and the absolute velocity as well as the angle of attack and sideslip as translational states $\begin{bmatrix} V & \alpha & \beta \end{bmatrix}^{\mathrm{T}}$.
The tail controlled missile model is actuated by four fins in cross-configuration and under nominal conditions the missile body has an axisymmetric configuration. Due to this symmetry a skid-to-turn policy can be utilized and the missile dynamics can be decoupled into separate sets of dynamic equations for pitch, roll and yawing motion [3]. Furthermore, in practical applications a single autopilot for acceleration tracking is designed, which is identical for the longitudinal and lateral motion. A third controller is then designed for stabilization of the roll attitude [3]. In the remainder of this paper only the longitudinal missile motion is considered for qLPV modeling and autopilot design. With $p = r = \beta = 0$ the nonlinear state equations (3) and (4) can then be written out for the two relevant short-period states α and q

$$\dot{\alpha} = \frac{\bar{q}S(-\sin(\alpha) \cdot C_{\mathrm{X}} + \cos(\alpha) \cdot C_{\mathrm{Z}}) - \cos(\alpha) \cdot T + mg_z^a}{mV} + q \tag{5}$$

$$\dot{q} = \frac{\bar{q}S(dC_m - \Delta x_{\mathrm{cg}} C_{\mathrm{Z}}) + (\dot{m}\Delta x_{\mathrm{cg/thrust}}^2 - \dot{I}_{yy}) \cdot q}{I_{yy}} \quad . \tag{6}$$

The aerodynamic coefficients are stored in lookup tables and are nonlinear dependent on Mach number Ma, incidence angle ϑ, elevator deflection η, pitch rate q and change of angle of attack $\dot{\alpha}$:

$$C_{\mathrm{X}} = f(Ma, \vartheta, \eta) \quad , \quad C_{\mathrm{Z}} = f(Ma, \vartheta, \eta) \quad , \quad C_{\mathrm{m}} = f(Ma, \vartheta, \eta, q, \dot{\alpha}) \quad . \tag{7}$$

The controlled variable is the longitudinal acceleration at the missile cg $a_{\mathrm{z,cg}}$, which is the total specific (non-gravitational) force divided by the missile mass. The measured outputs available for autopilot design are the angular rates and accelerations from an inertial measurement unit (IMU), resulting in an additional Euler acceleration term proportional to the lever arm l between the missile cg and IMU location:

$$a_{\mathrm{z,IMU}} = \frac{Z_{\mathrm{A}}^b + Z_{\mathrm{T}}^b}{m} + l \cdot \dot{q} \quad . \tag{8}$$

2.2 quasi-LPV Missile Model

There are different methods available in the literature to derive qLPV models from a system's nonlinear description. Although not necessarily providing the best approximation of the underlying nonlinear dynamics, a grid-based Jacobian linearization approach is the most common, as it can be directly generated for almost all types of nonlinear systems [6]. Depending on the chosen LPV controller synthesis approach, the LPV plant model $\boldsymbol{G}(s, \boldsymbol{\theta})$ must be given in the form of (1) with the state-space matrices of $\boldsymbol{G}(s, \boldsymbol{\theta})$ being affine functions with respect to the parameter vector $\boldsymbol{\theta}$. This kind of plant model is needed to derive a linear fractional representation (LFR) or polytopic LPV model. As has been shown in [17] and [18] the well-known $\mathcal{H}_\infty$ loop shaping approach from Glover and McFarlane [19] can directly be extended to polytopic LPV systems. For some systems such affine models can directly be derived from the nonlinear ones, e.g. by function substitution or state transformation. Examples can be found in [20]

for a variable stiffness actuator and in [5, 8, 9] for a wide-spread simplified missile model from [21, 22], which has explicit analytic expressions for the aerodynamic coefficients. For realistic aerospace applications the aerodynamic coefficients are nonlinear functions of different input variables and typically stored in numeric, multi-dimensional tables. Then, the most straightforward approach is to define a grid of k trim points and perform a numerical linearization of the nonlinear model around those trim points. The resulting grid-based LPV model is then represented by an array of k state-space models

$$\boldsymbol{G}_k(s) \overset{s}{=} \left[\begin{array}{c|c} \boldsymbol{A}_k & \boldsymbol{B}_k \\ \hline \boldsymbol{C}_k & \boldsymbol{D}_k \end{array}\right] \quad . \tag{9}$$

In [23] a rigorous approach is presented to generate affine LPV models from a grid-based description by performing successive steps of physical model analysis, possible simplifications and subsequent multivariable polynomial fitting. Here, a grid-based qLPV model of the missile is used to design an LPV controller based on the methods made available by the *LPVTools* software collection [10].

The linearized short-period dynamics of the missile in general form are given by

$$\begin{aligned} \begin{bmatrix} \dot{\alpha} \\ \dot{q} \end{bmatrix} &= \begin{bmatrix} Z_\alpha & 1 \\ M_\alpha & M_q \end{bmatrix} \cdot \begin{bmatrix} \alpha \\ q \end{bmatrix} + \begin{bmatrix} Z_\eta \\ M_\eta \end{bmatrix} \cdot \eta \\ \begin{bmatrix} q \\ a_{\mathrm{z,cg}} \\ a_{\mathrm{z,IMU}} \end{bmatrix} &= \begin{bmatrix} 0 & 1 \\ \bar{Z}_\alpha & 0 \\ \bar{Z}_\alpha - l \cdot M_\alpha & -l \cdot M_q \end{bmatrix} \cdot \begin{bmatrix} \alpha \\ q \end{bmatrix} + \begin{bmatrix} 0 \\ \bar{Z}_\eta \\ \bar{Z}_\eta - l \cdot M_\eta \end{bmatrix} \cdot \eta \end{aligned} \tag{10}$$

with the dimensional derivatives, i.e. the entries of the state-space matrices, being functions of different trim variables including "trimmed" mass flow rate during motor burn. An analytic description for (10) has been derived and reads, e.g., for the derivatives Z_α and M_q (the index "0" is used for trimmed variables):

$$Z_\alpha = \frac{\bar{q}_0 S}{m_0 V_0}(-\sin(\alpha_0)C_{X_\alpha,0} - \cos(\alpha_0)C_{X,0} + \cos(\alpha_0)C_{Z_\alpha,0} - \sin(\alpha_0)C_{Z,0}) - \cos(\alpha_0)T_0 \tag{11}$$

$$M_q = \frac{\bar{q}_0 S d^2}{I_{yy,0} V_0}(C_{m_q,0} + C_{m_{\dot{\alpha}},0}) + \frac{\dot{m}_0 \Delta x^2_{\mathrm{cg/thrust}} - \dot{I}_{yy,0}}{I_{yy,0}} \quad . \tag{12}$$

Prior to defining the parameter vector $\boldsymbol{\theta}$ a sensitivity analysis has been performed based on a semi-analytic linearization approach. A grid of trim points within the missile's flight envelope has been determined using *MATLAB's* `findop` command, witch each trim point being defined by a specific Mach number, altitude, angle of attack and burn phase, i.e. mass and cg configuration. Based on the resulting trim variables the dimensionless aerodynamic derivatives ($C_{m_\alpha}, C_{Z_\alpha}, \dots$) have been determined for each trim point by numerical perturbation of multivariabe look-up tables using the `linmod` command and inserted into the analytical description of (10), which was previously verified by comparison with numerical linearization of the complete short-period dynamics. This way different levels of simplification for the linearized short-period dynamics $\hat{G}_k(s)$ could be evaluated and compared to the nominal system $G_k(s)$ in order to identify certain effects, possibly during boost, which can be neglected. These studies can be considered as preliminary work for deriving affine model descriptions with minimal complexity. The ν-gap metric has been used as a measure of distance between two systems $\delta_\nu(\hat{G}_k(s), G_k(s))$ [24]. By evaluating a fine grid of 5904 trim points it turned out that the effects due to thrust and trimmed axial/longitudinal force coefficients can be neglected with a maximum of $\delta_{\nu,\max} = 0.14$ over all trim points and a mean of $\delta_{\nu,\mathrm{mean}} = 3.6e-2$.

To derive a grid-based qLPV model of the considered dual pulse missile first a choice regarding the elements of the parameter vector $\boldsymbol{\theta} = \left[\theta_1, \dots, \theta_p\right]^{\mathrm{T}} \in \mathbb{R}^p$ has to be made. This choice is not unique and

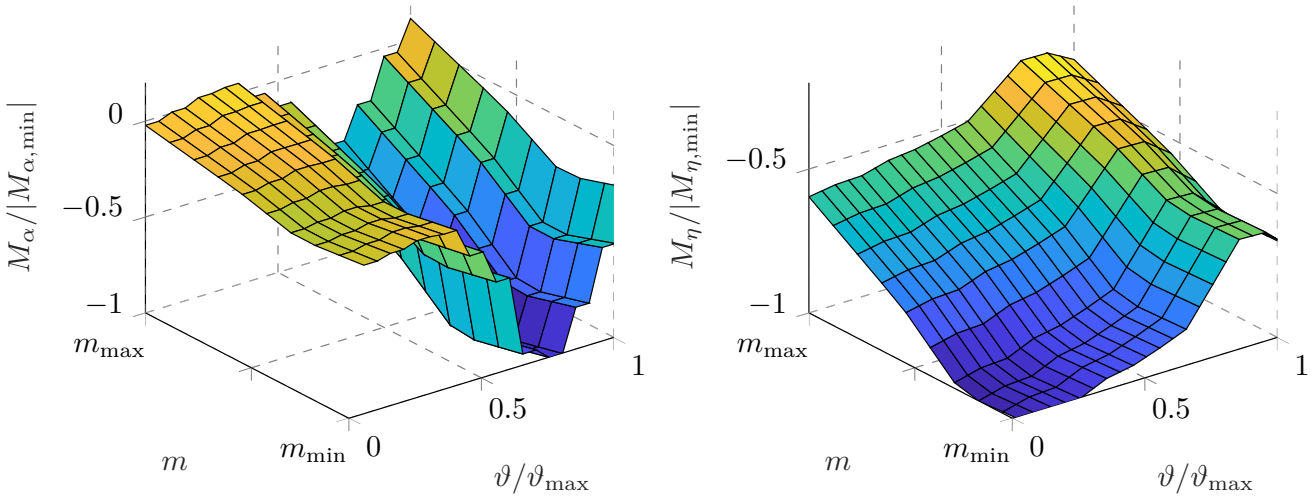

Fig. 1 Dimensional derivatives M_α (left) and M_η (right) over incidence angle ϑ and missile mass m for a fixed sub-sonic Mach number.

strongly depends on the required maneuverability, operational range and model fidelity. In most works on qLPV missile models scheduling is performed based on (absolute) angle of attack and Mach number [9, 15] while others also include altitude dependency [11]. As mentioned before, in this work the effects of relevant changes in mass and center of gravity position, which are unavoidable for a solid-fuel rocket motor, are also assessed. Here, the Mach number is also used as part of the parameter vector. Due to the high maneuverability of the missile the incidence angle ϑ is also considered as scheduling parameter with $\vartheta \in [0, \vartheta_{\max}]$. The choice of ϑ instead of α is legitimate due to the missile's axisymmetry. Analogous to the previous analyses the ν-gap metric between the elements $G_k(s)$ with $\vartheta = 0$ and $\vartheta = \vartheta_{\max}$ has been determined over the grid of trim points to justify the addition of ϑ to $\boldsymbol{\theta}$. Indeed, with $\delta_{\nu,\max} = 0.79$ and $\delta_{\nu,\text{mean}} = 0.69$ it implies conservatism if a controller $\boldsymbol{K}_k(s)$ at some grid point would need to robustly stabilize the missile over the whole incidence range. This is because of the relevant changes of the derivatives M_η and M_α in dependency of ϑ which are shown in figure 1 for a fixed sub-sonic Mach number[1]. The influence of the mass on the missile dynamics becomes more clear when looking at figure 2, where the course of the short period poles p_i and zeros z_i are shown for $m_{\max}$ and $m_{\min}$ over Mach number and for a fixed, low incidence angle. While the absolute values of the zeros are quite similar, the poles

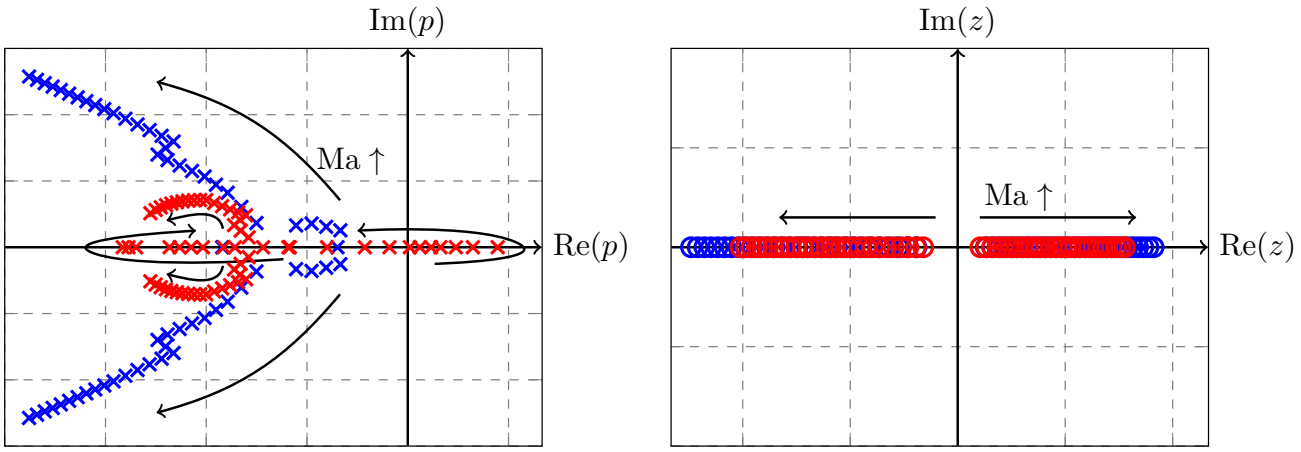

Fig. 2 Comparison of short period poles p_i (left) and zeros z_i (right) for minimum (—) and maximum (—) missile mass over Mach number for a fixed, low incidence angle ϑ.

[1]for confidentiality reasons all values shown in this paper are normalized to their respective maximum values

differ greatly. For the start configuration the dynamics are unstable at low Mach numbers, the burnt out configuration is always stable and has a natural frequency multiple times higher than during start. This difference is mainly due to the cg shift, which is implicit in the change of mass. When recalling that the condition $M_\alpha < 0$ is necessary for static stability (see e.g. [16]) it becomes clear that for aft cg positions where M_α is positive the short-period dynamics become unstable. Finally, the question arises whether both the mass and the center of gravity position should be added as elements of $\boldsymbol{\theta}$, as was done in [25] for an aircraft model. Due to the direct correlation between mass and cg position for a solid-fuel missile, the addition of the mass is considered sufficient here. Thus, the parameter vector is given by

$$\boldsymbol{\theta} = \begin{bmatrix} Ma & \vartheta & m \end{bmatrix} \quad . \tag{13}$$

Although altitude or respectively air density ρ could also be added to $\boldsymbol{\theta}$, it is accounted for by proper scaling of the controller gains as proposed in [26]. This is due to the approximate proportionality of the short-period dynamics to ρ. Therefore, the qLPV model is derived at sea level altitude. The parameter vector $\boldsymbol{\theta}$ contains 6 grid points for the Mach number, 7 for the incidence angle and 3 for the mass. For validation of the qLPV model first frequency responses at a number of grid points have been compared to those of the original LTI models at those points, showing no difference. Then, frequency responses of the LPV model between two neighboring grid points have been evaluated and compared to the corresponding LTI models to check consistency of the performed interpolation. Again, the model showed consistent behavior. Finally, the qLPV model has been compared to the nonlinear dynamics. Figure 3 shows a comparison of the longitudinal acceleration $a_{z,cg}$ and pitch rate q in response to four equal elevator doublette commands while burning both motor pulses and passing through the flight envelope. The altitude has been fixed at sea level. While the transient behavior does not accurately match at the start of the first pulse, the qLPV model approximates the nonlinear dynamics quite well for the rest of the simulation.

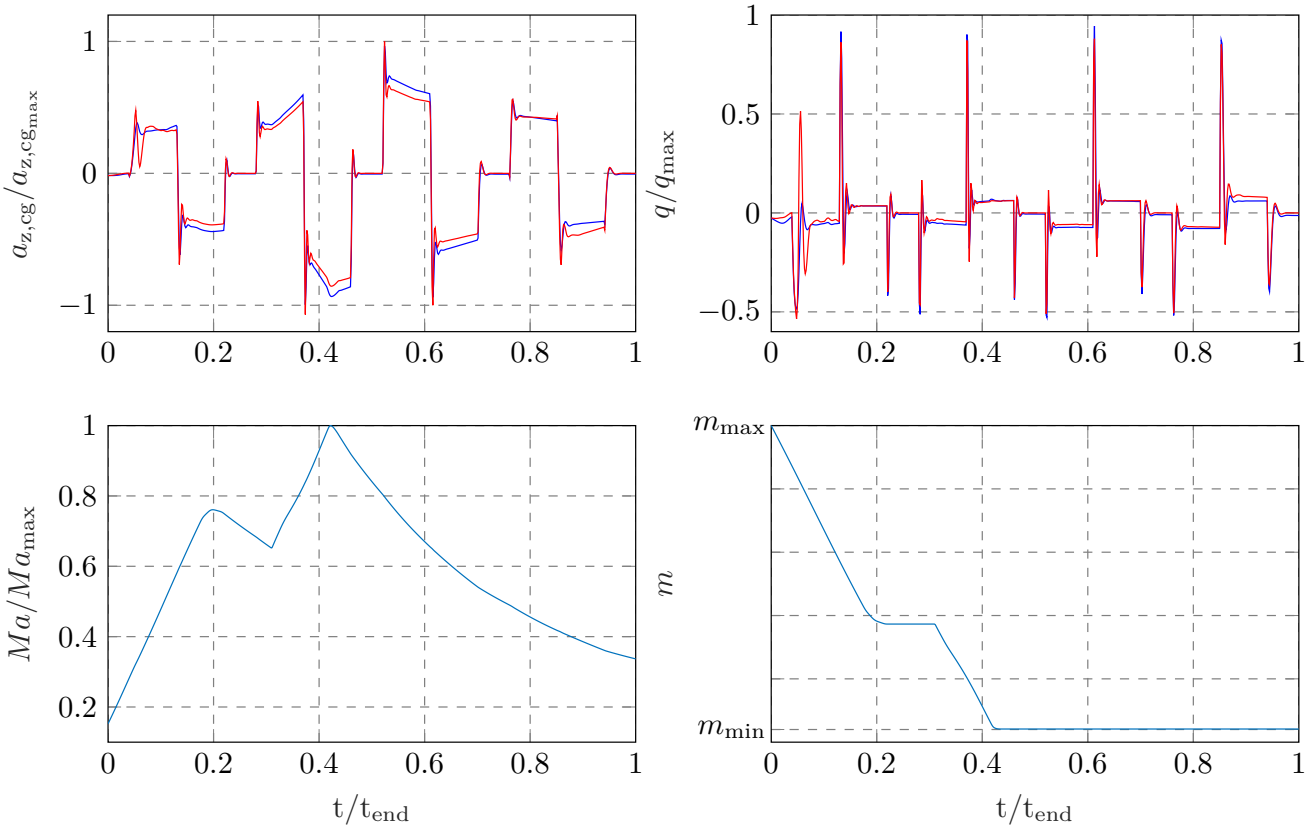

Fig. 3 Comparison of the nonlinear (—) and qLPV missile model (—) fixed at sea level altitude.

3 LPV Controller Design

This section describes the synthesis of a robust LPV autopilot for the missile longitudinal dynamics. After a brief summary of the theoretical background on the $\mathcal{L}_2$-induced control framework, the design of the controller is summarized. This includes a description of the considered design model and the choice of weighting functions to include robustness and performance requirements.

3.1 Induced $\mathcal{L}_2$-norm Controller Design

The setup for LPV controller design can be viewed as an extension to the $\mathcal{H}_\infty$-framework and is depicted in figure 4. $\boldsymbol{P}(s,\boldsymbol{\theta})$ is the generalized LPV plant with

$$\begin{bmatrix} \dot{\boldsymbol{x}} \\ \boldsymbol{z} \\ \boldsymbol{y} \end{bmatrix} = \underbrace{\left[\begin{array}{c|cc} \boldsymbol{A}(\boldsymbol{\theta}) & \boldsymbol{B}_1(\boldsymbol{\theta}) & \boldsymbol{B}_2(\boldsymbol{\theta}) \\ \hline \boldsymbol{C}_1(\boldsymbol{\theta}) & \boldsymbol{D}_{11}(\boldsymbol{\theta}) & \boldsymbol{D}_{12}(\boldsymbol{\theta}) \\ \boldsymbol{C}_2(\boldsymbol{\theta}) & \boldsymbol{D}_{21}(\boldsymbol{\theta}) & \boldsymbol{D}_{22}(\boldsymbol{\theta}) \end{array}\right]}_{\boldsymbol{P}(s,\boldsymbol{\theta})} \cdot \begin{bmatrix} \boldsymbol{x} \\ \boldsymbol{w} \\ \boldsymbol{u} \end{bmatrix} \quad . \tag{14}$$

The signals $\boldsymbol{u}$ are the control variables, $\boldsymbol{y}$ the measured variables, $\boldsymbol{w}$ the performance inputs and $\boldsymbol{z}$ performance outputs. Performance specifications for the controller are formulated in terms of the induced $\mathcal{L}_2$-norm which, for a given LPV system $\boldsymbol{G}(\boldsymbol{\theta})$, is defined as (see e.g. [10, 27])

$$||\boldsymbol{G}(\boldsymbol{\theta})||_{i,2} = \sup_{\boldsymbol{w}\in\mathcal{L}_2, ||\boldsymbol{w}||_2\neq 0} \frac{||\boldsymbol{z}||_2}{||\boldsymbol{w}||_2} = \sup_{\boldsymbol{w}\in\mathcal{L}_2, ||\boldsymbol{w}||_2\neq 0} \frac{||\boldsymbol{G}(\boldsymbol{\theta})\boldsymbol{w}||_2}{||\boldsymbol{w}||_2} \quad . \tag{15}$$

For a fixed parameter vector $\boldsymbol{\theta}$ = const the norm coincides with the $\mathcal{H}_\infty$-norm. The optimization problem for designing the LPV controller $\boldsymbol{K}(s,\boldsymbol{\theta})$ is given by

$$\min_{\boldsymbol{K}(s,\boldsymbol{\theta})} ||F_l(\boldsymbol{P}(s,\boldsymbol{\theta}), \boldsymbol{K}(s,\boldsymbol{\theta}))||_{i,2} \tag{16}$$

where $F_l(.,.)$ describes the lower linear fractional transformation (LFT) shown in figure 4. As in classical $\mathcal{H}_2/\mathcal{H}_\infty$ control the resulting LPV controller has the same number of states as the generalized plant $\boldsymbol{P}(s,\boldsymbol{\theta})$. It includes the LPV plant model as well as the designer-specified weighting functions. The choice of weighting functions for the missile autopilot is described in the next section.
In contrast to classical gain scheduling, which is limited to systems with slow parameter variation rates [28], the LPV design framework is also able to take fast varying scheduling parameters, like the incidence angle, into account [27]. If bounded (symmetric) parameter rates $|\dot{\boldsymbol{\theta}}| < \boldsymbol{\nu}$ are incorporated in the controller design, it is possible to receive less conservative results as for a controller that needs to consider arbitrary fast changes in $\boldsymbol{\theta}$ [15]. The function `lpvsyn` from the *LPVTools* software package allows to either synthesize rate-unbounded or rate-bounded LPV controllers [10]. In [27] the underlying LPV

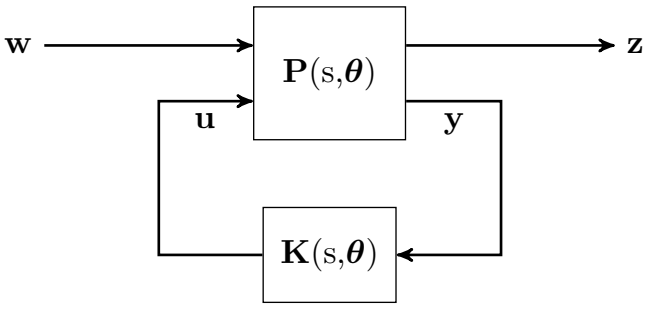

Fig. 4 Generalized plant $\boldsymbol{P}(s,\boldsymbol{\theta})$ for LPV controller design.

synthesis problem is formulated in terms of the induced $\mathcal{L}_2$-norm by applying a generalized version of the Bounded Real Lemma. In short, it states that an LPV system $\boldsymbol{G}(s,\boldsymbol{\theta})$ with $\boldsymbol{\theta} \in \mathcal{P} \subseteq \mathbb{R}^{n_p}$ and $|\dot{\boldsymbol{\theta}}| < \boldsymbol{\nu}$ is exponentially stable and $||\boldsymbol{G}(\boldsymbol{\theta})||_{i,2} < \gamma$ for all $\boldsymbol{\theta} \in \mathcal{P}$ subject to $|\dot{\boldsymbol{\theta}}| < \boldsymbol{\nu}$ if there exists an $\boldsymbol{X}(\boldsymbol{\theta}) > \boldsymbol{0}$ such that

$$\begin{bmatrix} \boldsymbol{A}^{\mathrm{T}}(\boldsymbol{\theta})\boldsymbol{X}(\boldsymbol{\theta}) + \boldsymbol{X}(\boldsymbol{\theta})\boldsymbol{A}(\boldsymbol{\theta}) + \sum_{i=1}^{n_p} \beta_i \frac{\delta \boldsymbol{X}(\boldsymbol{\theta})}{\delta \theta_i} & \boldsymbol{X}(\boldsymbol{\theta})\boldsymbol{B}(\boldsymbol{\theta}) & \gamma^{-1}\boldsymbol{C}^{\mathrm{T}}(\boldsymbol{\theta}) \\ \boldsymbol{B}^{\mathrm{T}}(\boldsymbol{\theta})\boldsymbol{X}(\boldsymbol{\theta}) & -\boldsymbol{I} & \gamma^{-1}\boldsymbol{D}^{\mathrm{T}}(\boldsymbol{\theta}) \\ \gamma^{-1}\boldsymbol{C}(\boldsymbol{\theta}) & \gamma^{-1}\boldsymbol{D}(\boldsymbol{\theta}) & -\boldsymbol{I} \end{bmatrix} < \boldsymbol{0} \tag{17}$$

where $|\beta_i| \leq \nu_i, i = 1, \ldots, n_p$. As the matrices $\boldsymbol{A}(\boldsymbol{\theta}), \boldsymbol{B}(\boldsymbol{\theta}), \boldsymbol{C}(\boldsymbol{\theta}), \boldsymbol{D}(\boldsymbol{\theta})$ and $\boldsymbol{X}(\boldsymbol{\theta})$ are continuous functions of the parameter vector $\boldsymbol{\theta}$, the set of linear matrix inequalities (LMIs) in condition (17) is infinite-dimensional [10]. The approximate solution implemented in `lpvsyn` is given by solving (17) over a finite grid for the k trim points from which the qLPV model has been designed. Therefore, a basis for $\boldsymbol{X}(\boldsymbol{\theta})$ has to be defined with a number of n_b basis functions, such that

$$\boldsymbol{X}(\boldsymbol{\theta}) = \sum_{j=1}^{n_b} f_j(\boldsymbol{\theta})\boldsymbol{X}_j \quad . \tag{18}$$

The basis functions should be chosen in accordance with the plants dependency on $\boldsymbol{\theta}$ [15]. In [29] a comparison showed that for the model of a large flexible aircraft affine basis functions gave the best trade-off between achievable performance and computational effort. For the rate-unbounded case ($\boldsymbol{\nu} = \infty$) the use of a constant, parameter independent matrix $\boldsymbol{X}(\boldsymbol{\theta}) = \boldsymbol{X}$ is sufficient. In summary, for the grid-based approach, the function `lpvsyn` needs to solve a total of $(k \cdot 2^{n_p} + 1)$ LMIs for γ and $\boldsymbol{X}_1, \ldots, \boldsymbol{X}_{n_b}$ [10].

3.2 LPV Missile Autopilot Synthesis

In this section the design procedure for the longitudinal LPV autopilot is described. Figure 5 shows the interconnection structure of the generalized plant $\boldsymbol{P}(s,\boldsymbol{\theta})$ that has been employed for controller synthesis. The design model consists of the second order short-period dynamics (10) which have been augmented with a second order model representing the actuator dynamics with the natural frequency ω_0 and damping factor D:

$$\begin{bmatrix} \dot{\eta} \\ \ddot{\eta} \end{bmatrix} = \begin{bmatrix} 0 & 1 \\ -\omega_0^2 & -2D\omega_0 \end{bmatrix} \begin{bmatrix} \eta \\ \dot{\eta} \end{bmatrix} + \begin{bmatrix} 0 \\ \omega_0^2 \end{bmatrix} \eta_{\mathrm{cmd}} \quad . \tag{19}$$

In addition, to model a time delay in the flight control computer the measured outputs of (10), i.e. the pitch rate q and longitudinal acceleration at the accelerometer $a_{\mathrm{z,IMU}}$, have been delayed by $n_d = 2$ samples using a first order Padé approximation as in [26]:

$$G_{\mathrm{delay}}(s) = e^{-n_d T_s s} \approx \frac{-n_d T_s s + 2}{n_d T_s s + 2} \quad . \tag{20}$$

The LPV controller $\boldsymbol{K}(s,\boldsymbol{\theta})$ has been designed in a (1,2) fashion with acceleration tracking and rate damping. The resulting controller is of 8th order. Bounds for the parameter variation rates have been estimated from nonlinear missile simulations and added to the short-period qLPV plant model such that $|\dot{M}a| < \nu_1$, $|\dot{\vartheta}| < \nu_2$ and $|\dot{m}| < \nu_3$. In total five weighting functions have been added to the generalized plant in order to implement input/output performance requirements in the design. As with conventional mixed-sensitivity or signal-based $\mathcal{H}_2/\mathcal{H}_\infty$ controller design weighting functions are used to impose requirements on closed-loop bandwidth, robustness, steady-state tracking error etc. [12]. The implemented weights are described in the following:

- As in [26] the constant weight $W_{\mathrm{a,cmd}}$ has been added to specify the ratio of acceleration tracking to rate damping loop.

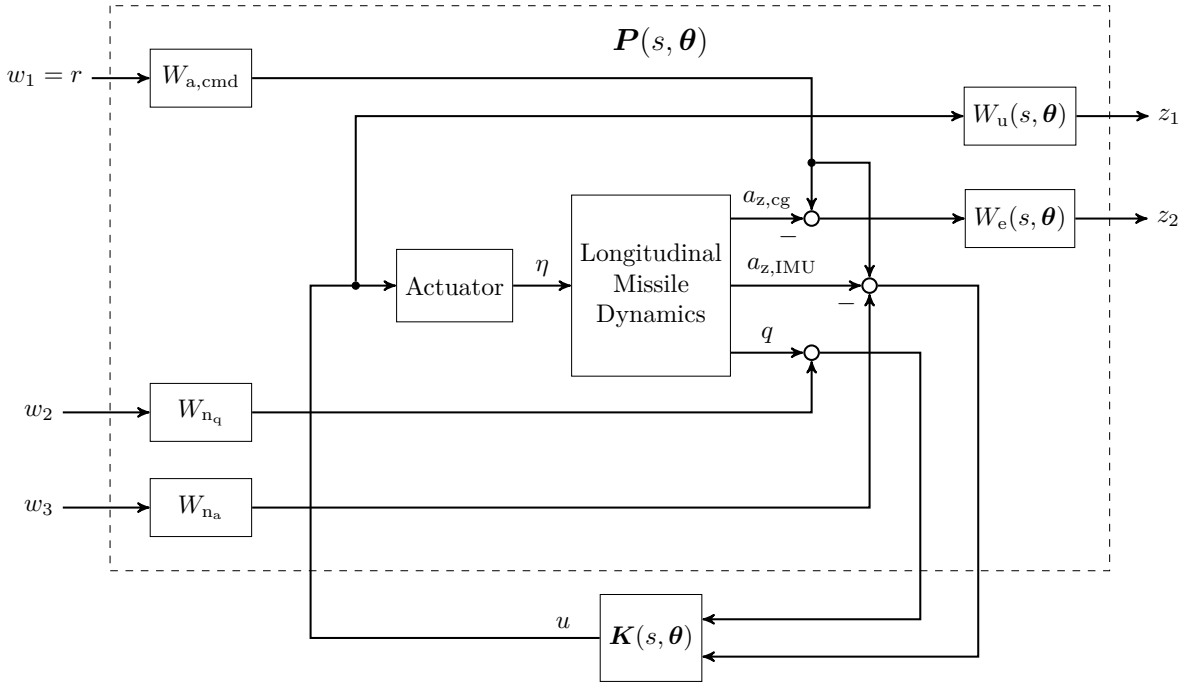

Fig. 5 Generalized plant for longitudinal LPV controller synthesis.

- The constant weights W_{n_q} and W_{n_a} are implemented to include the influence of sensor noise in the design. Their values have been chosen based on the noise characteristics of the IMU model implemented in a full 6DoF simulation.
- The weight $W_u(s,\boldsymbol{\theta})$ is added to limit actuator bandwidth and thus ensuring robustness against high frequency disturbances. It is implemented in a first-order high pass structure:

$$W_u(s,\boldsymbol{\theta}) = \frac{1}{M_u(\boldsymbol{\theta})} \cdot \frac{s}{s+\omega_u(\boldsymbol{\theta})} \quad . \tag{21}$$

- The weight $W_e(s,\boldsymbol{\theta})$ has been implemented as a parameter-dependent first order lag-like structure to specify the steady-state error and closed-loop bandwidth [12]:

$$W_e(s,\boldsymbol{\theta}) = \frac{\frac{1}{M_e(\boldsymbol{\theta})}s + \omega_e(\boldsymbol{\theta})}{s + \omega_e(\boldsymbol{\theta}) \cdot A_e(\boldsymbol{\theta})} \quad , \quad A_e(\boldsymbol{\theta}) < M_e(\boldsymbol{\theta}) \quad . \tag{22}$$

Tuning the LPV weights over the parameter grid can be a tedious task, e.g. in [15] an optimization procedure based on requirements regarding rise time, settling time, overshoot and other metrics has been introduced. To simplify the design task here the parameters of $W_u(s,\boldsymbol{\theta})$ have been chosen to be constant. The parameters A_e and M_e have also been fixed, representing a bound on steady-state error and peak sensitivity respectively. Finally, the frequency $\omega_e(\boldsymbol{\theta})$ has been scheduled based on a simple constraint on the sensitivity bandwidth by limiting it to be a fraction of the non-minimum phase zero of the k-th grid transfer function $G_k(s) = \frac{a_{\mathrm{z,cg}}(s)}{\eta(s)}$, which poses a fundamental limitation for achievable closed-loop performance [12]. This can be interpreted as a surrogate requirement for the closed-loop rise time. The final values for $\omega_e(\boldsymbol{\theta})$ at each grid point were determined from the respective results from a local $\mathcal{H}_\infty$ controller design as proposed in [15]. Figure 6 shows the resulting demands for sensitivity bandwidth ω_{S} over Mach number, incidence and missile mass, scaled to the maximum value $\omega_{\mathrm{S,max}}$ which can be achieved in burnt out state at the maximum Mach number and incidence. The small change over mass is due to the similar zero locations for $m_{\max}$ and $m_{\min}$ which have been shown in section 2.2. The fundamentally different stability properties of the plant generally lead to the demand of a sufficient low gain of $S(j\omega)$ below ω_e for unstable cases. Here, the DC gain A_e has been set to 40 dB.

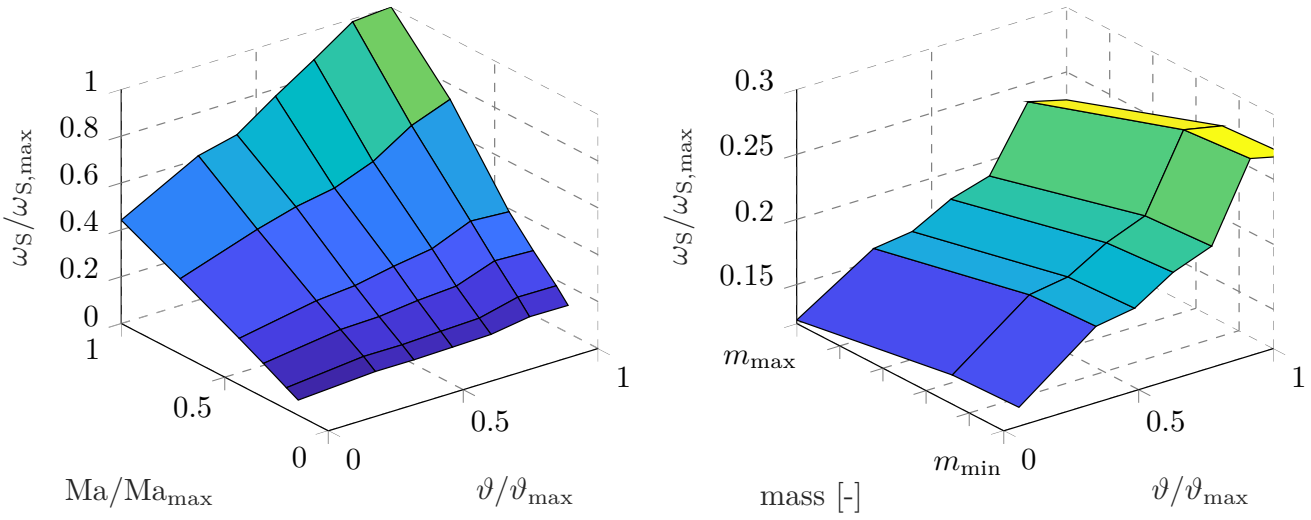

Fig. 6 Demand for sensitivity bandwidth over incidence and Mach number (left) and over incidence and missile mass (right), scaled to the maximum achievable value $\omega_{S,max}$.

After some trials the basis functions have been chosen to be affine in the elements of $\boldsymbol{\theta}$:

$$\boldsymbol{X}(\boldsymbol{\theta}) = \boldsymbol{X}_1 + Ma \cdot \boldsymbol{X}_2 + \vartheta \cdot \boldsymbol{X}_3 + m \cdot \boldsymbol{X}_4 \quad . \tag{23}$$

The robustness and performance of the LPV controller are assessed in the following section.

4 Robustness and Performance Analysis

In this section robust stability and performance of the closed-loop system is investigated. Linear analysis techniques are used to assess the robustness properties at selected trim points within the flight envelope. Finally, the LPV autopilot's performance is analyzed within a high-fidelity nonlinear simulation environment.

4.1 Linear Robustness Analysis

To analyze the robustness of the developed LPV controller a μ-analysis has been performed at all 126 grid points within the missile's flight envelope. The design model has been augmented with a diagonal parametric uncertainty block, introducing 10% uncertainty for the dimensional derivatives of the short-period model, as well as 10% uncertainty for the actuator's natural frequency. This accounts for variations in the aerodynamics e.g. due to dependencies on the trimmed virtual elevator deflection η and inaccuracies in the estimation of the scheduling variables, which are not directly available for measurement. Figure 7 shows the maximum structured singular value over all frequencies at each grip point for the empty and full missile, respectively. As can be seen the LPV controller robustly stabilizes the empty missile at each grid point with the maximum value $\mu_{max} = 0.85$ occuring at a transonic Mach number and medium incidence angle. For the full missile, however, there are four grid points for which $\mu_{max} > 1$ with the maximum of 1.2 occuring at a similar combination of incidence angle and Mach number as for the endgame configuration. For both worst-case values of μ_{max} the underlying open-loop plant model is stable. Figure 7 also shows the structured singular values for both of these grid points over the frequency. As can be seen, the qualitative course of the upper and lower structure singular value is very similar, with the absolute maximum μ_{max} occuring in both cases around 15 rad s^{-1}. Further sensitivity analyses have shown that the peak μ_{max} is primarily caused by the uncertainty in M_η at both grid points.
Practically, the four outliers with $\mu_{max} > 1$ don't pose a problem as they correspond to Mach numbers

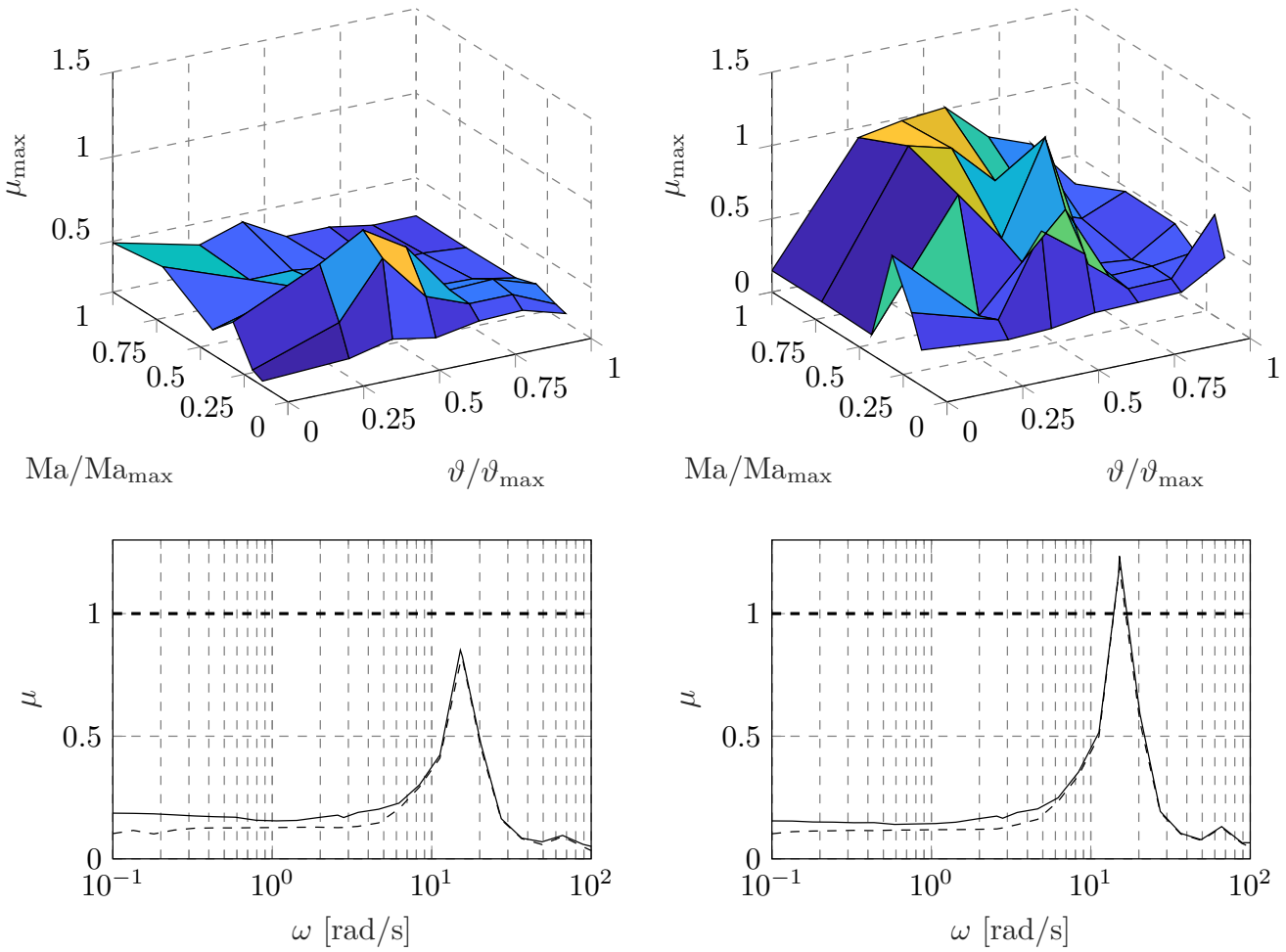

Fig. 7 Top: Maximum structured singular value over all frequencies for empty (left) and full missile (right). Bottom: Structured singular values at worst-case grid points for empty (left) and full missile (right).

which cannot be reached for the start configuration with maximum mass. For the intermediate mass grid point the missile is robustly stabilized for all combinations of Mach number and incidence (not shown).

4.2 Nonlinear Simulation Results

The autopilot performance has been assessed by conducting nonlinear simulations. The LPV controller has been implemented in a 6DoF simulation model of the missile with the lateral and roll channel frozen to evaluate the pure longitudinal motion. The altitude has also been fixed to sea level at which the qLPV model was derived and the LPV controller has been synthesized. The simulation model includes the full nonlinear aerodynamics, a motor model, a detailed model of the control section as well as an IMU model. The latter includes typical sensor dynamics, lever arm effects, i.e. Euler and centripetal acceleration due to the IMU being displaced from the cg, and sensor errors. For the performance assessment the actuators' natural frequency as well as all aerodynamic coefficients, which consist of a base and a control increment part, have been varied in the range of ±10%. Control response simulations have been performed by commanding subsequent acceleration doublette commands to the autopilot while the two motor pulses are burned and missile velocity changes rapidly. The scheduling parameters are assumed to be measurable but must be estimated in reality. In total 200 simulations have been performed to investigate the robustness of the qLPV controller against the considered uncertainties while covering the whole flight envelope from the start to the endgame configuration. Figure 8 shows the results of the simulations. The c.g. acceleration of the missile ($a_{z,cg}$) has been normalized to the commanded acceleration amplitude while the elevator deflection (η) has been scaled to it's physical deflection limit. Here, only the

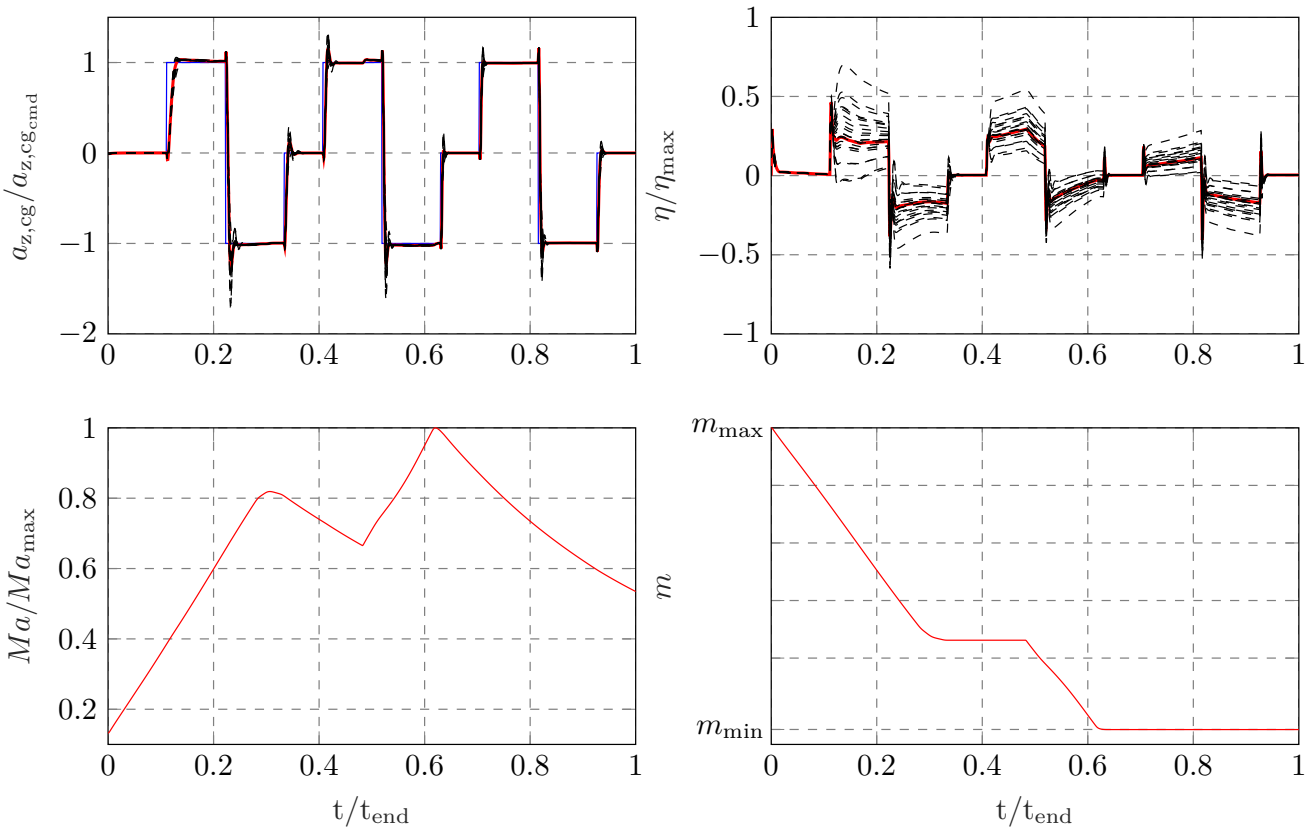

Fig. 8 Tracking response of the nominal (—) and uncertain (—) nonlinear missile model to doublette acceleration commands (—).

results from 20 simulations runs are plotted including the worst-case deviations from the nominal tracking behaviour. As can be seen, the qLPV autopilot stabilizes the missile robustly over the entire envelope with good overall tracking behaviour and only slight performance degradation due to uncertainties. The worst-case overshoot lies in the range of 35% and occurs in a very agile region of the flight envelope, i.e. at a high Mach number and after the first pulse has burned out.

5 Conclusion and Future Works

In this work a robust LPV autopilot has been designed for the model of a high-agile dual pulse surface-to-air missile. First, a quasi-LPV model of the missile has been derived with special attention to the effects of mass reduction and center of gravity shift whose influence on the dynamics turned out to be very relevant. Second, an LPV controller for longitudinal acceleration tracking has been designed based on the induced $\mathcal{L}_2$-norm control framework. The resulting LPV controller is synthesized over a grid of trim points for different Mach numbers, incidence angles and missile masses with an a-posteriori scheduling over air density [26]. Linear robustness analyses were carried out over the grid points of the flight envelope with the closed control loop showing good robustness to aerodynamic uncertainties. The autopilot also showed good tracking behavior within a nonlinear high-fidelity simulation environment. Future work will focus on improving closed-loop performance by employing additional LPV feedforward control and optimizing LPV weighting functions. It is planned to extend the autopilot by implementing a full skid-to-turn steering policy. Also, anti-windup measures need to be integrated and the influence of body-bending dynamics will be assessed.

References

[1] F. Nesline and P. Zarchan. Robust instrumentation configurations for homing missile flight control. In *Guidance and Control Conference*, page 1749, 1980.

[2] W. J. Rugh and J. S. Shamma. Research on gain scheduling. *Automatica*, 36(10):1401–1425, 2000.

[3] H. Buschek. Full envelope missile autopilot design using gain scheduled robust control. *Journal of Guidance, Control, and Dynamics*, 22(1):115–122, 1999.

[4] B. J. E. Misgeld, R. Dold, T. Kuhn, and H. Buschek. Robust autopilot design for a high-agile ground-to-air missile. DGLR-Jahrestagung, Hamburg, 2010.

[5] J.-M. Biannic and P. Apkarian. Missile autopilot design via a modified lpv synthesis technique. *Aerospace Science and Technology*, 3(3):153–160, 1999.

[6] A. Marcos and G. J. Balas. Development of linear-parameter-varying models for aircraft. *Journal of Guidance, Control, and Dynamics*, 27(2):218–228, 2004.

[7] J. S. Shamma and J. R. Cloutier. Gain-scheduled missile autopilot design using linear parameter varying transformations. *Journal of guidance, Control, and dynamics*, 16(2):256–263, 1993.

[8] P. C. Pellanda, P. Apkarian, and H. D. Tuan. Missile autopilot design via a multi-channel lft/lpv control method. *International Journal of Robust and Nonlinear Control: IFAC-Affiliated Journal*, 12(1):1–20, 2002.

[9] F. Wu, A. Packard, and G. Balas. Systematic gain-scheduling control design: A missile autopilot example. *Asian Journal of Control*, 4(3):341–347, 2002.

[10] A. Hjartarson, P. Seiler, and A. Packard. Lpvtools: A toolbox for modeling, analysis, and synthesis of parameter varying control systems. *IFAC-PapersOnLine*, 48(26):139–145, 2015.

[11] P. Apkarian, P. Gahinet, and G. Becker. Self-scheduled h∞ control of linear parameter-varying systems: a design example. *Automatica*, 31(9):1251–1261, 1995.

[12] S. Skogestad and I. Postlethwaite. *Multivariable feedback control: analysis and design*. john Wiley & sons, 2005.

[13] F. Wu, X. H. Yang, A. Packard, and G. Becker. Induced l2-norm control for lpv systems with bounded parameter variation rates. *International Journal of Robust and Nonlinear Control*, 6(9-10):983–998, 1996.

[14] G. Becker. *Quadratic stability and performance of linear parameter dependent systems*. University of California, Berkeley, 1993.

[15] H. Pfifer and S. Hecker. Lpv controller synthesis for a generic missile model. In *2010 IEEE International Conference on Control Applications*, pages 1838–1843. IEEE, 2010.

[16] B. L. Stevens, F. L. Lewis, and E. N. Johnson. *Aircraft control and simulation: dynamics, controls design, and autonomous systems*. John Wiley & Sons, 2015.

[17] P. Apkarian, J.-M. Biannic, and P. Gahinet. Self-scheduled h-infinity control of missile via linear matrix inequalities. *Journal of Guidance, Control, and Dynamics*, 18(3):532–538, 1995.

[18] E. Prempain. Gain-scheduling h∞ loop shaping control of linear parameter-varying systems. *IFAC Proceedings Volumes*, 39(9):215–219, 2006.

[19] D. McFarlane and K. Glover. A loop-shaping design procedure using h/sub infinity/synthesis. *IEEE transactions on automatic control*, 37(6):759–769, 1992.

[20] L. Bergmann, L. Liu, N. Pham, B. Misgeld, S. Leonhardt, and C. Ngo. Implementation of lpv h∞ loop-shaping control for a variable stiffness actuator. *IFAC-PapersOnLine*, 53(2):10129–10134, 2020.

[21] R. T. Reichert. Robust autopilot design using μ-synthesis. In *1990 American Control Conference*, pages 2368–2373. IEEE, 1990.

[22] R. A. Nichols, R. T. Reichert, and W. J. Rugh. Gain scheduling for h-infinity controllers: A flight control example. *IEEE Transactions on Control systems technology*, 1(2):69–79, 1993.

[23] H. Pfifer and S. Hecker. Generation of optimal linear parametric models for lft-based robust stability analysis and control design. *IEEE Transactions on Control Systems Technology*, 19(1):118–131, 2010.

[24] G. Vinnicombe. *Uncertainty and Feedback, H Loop-shaping and the V-gap Metric*. World Scientific, 2000.

[25] S. Hecker and H. Pfifer. Affine lpv-modeling for the addsafe benchmark. *Control Engineering Practice*, 31:126–134, 2014.

[26] B. J. E. Misgeld, M. Darcis, and T. Kuhn. Robust linear-parameter varying autopilot design for a tail/thrust vector controlled missile. In *Advances in Aerospace Guidance, Navigation and Control: Selected Papers of the 1st CEAS Specialist Conference on Guidance, Navigation and Control*, pages 287–301. Springer, 2011.

[27] F. Wu. *Control of linear parameter varying systems*. University of California, Berkeley, 1995.

[28] D. J. Leith and W. E. Leithead. Survey of gain-scheduling analysis and design. *International journal of control*, 73(11):1001–1025, 2000.

[29] J. Theis, H. Pfifer, G. Balas, and H. Werner. Integrated flight control design for a large flexible aircraft. In *2015 American Control Conference (ACC)*, pages 3830–3835. IEEE, 2015.